Synthesis of a Novel n-Type Conducting Polymer and Its Applications for Enhanced Perovskite Stability

A Thesis

submitted to

Indian Institute of Science Education and Research Pune in partial fulfilment of

the requirements for the BS-MS Dual Degree Programme

By

Yadram Meena

(20191207)

Indian Institute of Science Education and Research Pune

Dr. Homi Bhabha Road, Pashan, Pune, 411008, INDIA.

April, 2024

Supervisor: Dr. Pabitra Kumar Nayak

Reader,

Tata Institute of Fundamental Research, Hyderabad

Certificate

This is to certify that this dissertation entitled "**Synthesis of a Novel n-Type Conducting Polymer and Its Applications for Enhanced Perovskite Stability**" towards the partial fulfilment of the BS-MS dual degree programme at the Indian Institute of Science Education and Research, Pune represents study/work carried out by "**Yadram Meena** at Tata Institute of Fundamental Research, Hyderabad" under the supervision of "**Dr. Pabitra Kumar Nayak**, Reader, Tata Institute of Fundamental Research, Hyderabad" during the academic year 2023-24.

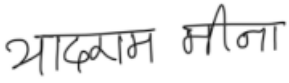

Student's signature

Date: 27/03/2024

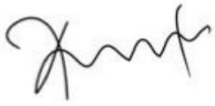

Supervisor's signature

Date: 25/03/2024

Declaration

I hereby declare that the matter embodied in the report entitled "**Synthesis of a Novel n-Type Conducting Polymer and Its Applications for Enhanced Perovskite Stability**" are the results of the work carried out by me at Tata Institute of Fundamental Research, Hyderabad, under the supervision of **Dr. Pabitra Kumar Nayak** and the same has not been submitted elsewhere for any other degree. Wherever others contribute, every effort is made to indicate this clearly, with due reference to the literature and acknowledgement of collaborative research and discussions.

Yadram Meena
20191207

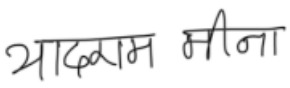

Student's signature

Date: 27/03/2024

This Thesis is dedicated to **my beloved Family…….**

Acknowledgements

I am deeply grateful for the support and guidance I received throughout my BS-MS project. My sincere thanks go to Dr. Pabitra Kumar Nayak for his mentorship, encouragement, and the freedom he granted me to explore my research interests. I also extend my gratitude to Prof. Ramanathan Vaidyanathan for his ongoing support and valuable suggestions. Their expertise helped me tremendously in refining my research approach and overall work.

Special thanks to Mr. Subham Gupta for teaching me essential laboratory techniques that have laid the foundation for my future research endeavours.

My lab-mates deserve recognition, especially Mr. Sagar, Mr. Brijesh and Dr. Sujit for their camaraderie and support. Our discussions and shared insights have been incredibly helpful.

Finally, my deepest gratitude goes to my parents, and my brother. Their unconditional love and belief in me have been my driving force. I couldn't have achieved this without them. To everyone who has played a role, big or small, in the successful completion of my five-year journey, I offer my sincerest thanks.

Contents

List of figures

List of Schemes

Abbreviations

MHPs	Metal Halide Perovskites
Cp	Conducting Polymer
HOMO	Highest occupied molecular orbital
LUMO	Lowest unoccupied molecular orbital
DMSO	Dimethyl Sulfoxide
HBFDO	Benzo[1,2-b:4,5-b′] difuran-2,6-dione
PBFDO	Poly(benzodifurandione)
KPM	Kelvin Probe Microscopy
XRD	X-ray Diffraction
NMR	Nuclear Magnetic Resonance
FTO	Fluorine-doped Tin Oxide
$FAPbI_3$	Formamidinium Lead Iodide
OPVs	Organic Photovoltaics
OLEDs	Organic Light emitting diodes
OFETs	Organic Field effect transistors

Abstract

Perovskite solar cells (PSCs) offer remarkable potential for low-cost, high-efficiency photovoltaics. However, their widespread adoption is hindered by long-term instability, particularly of the widely studied $FAPbI_3$ composition. Additionally, the development of stable and efficient n-type conducting polymers (CPs) remains a challenge in organic electronics. This thesis addresses both issues through the synthesis of a highly conductive n-type polymer and its application in stabilizing $FAPbI_3$ perovskites.

A simplified method for synthesizing poly(benzodifurandione) (PBFDO), a known n-type CP, was established. The polymer's electrical conductivity and mechanism were thoroughly characterized. Caesium salt of PBFDO was then strategically combined with $FAPbI_3$ to create mixed-cation, multi-component perovskite composites. Complete structural analysis (XRD, SEM, Uv-Vis) revealed the polymer's influence on perovskite crystal formation and morphology.

Importantly, these PBFDO-containing perovskite composites exhibited significantly improved stability under ambient conditions and improved film morphology compared to pure $FAPbI_3$. This work highlights the potential of n-type conducting polymers to unlock new approaches for enhancing perovskite solar cell stability while simultaneously contributing to the development of advanced organic electronic materials.

1. Introduction

1.1 Chapter 1: Conducting Polymers

Polymers are large molecules (also known as macromolecules) formed by linking smaller units (monomers) in diverse ways. This linking process results in various patterns, like straight lines, branches, or complex networks. Polymers have long been used as insulators, as they don't typically conduct electricity. However, a 1977 study by Hediki Shirikawa, Alan Macdiarmid, and Allan Heeger revealed that organic materials, especially polyacetylene [1], could behave like metals or semiconductors. These conductive polymers offer a unique combination: low cost, light weight, toughness, and ease of fabrication, alongside their surprising electrical properties. These polymers often have interconnected poly-conjugated structures. In their initial form, they act as insulators, but when chemically modified (through oxidation or reduction), they can be converted into conductive polymer salts with electrical conductivities similar to Metals and semiconductors.

Conducting polymers are unique due to their extended system of connected atoms with alternating single and double bonds. This 'conjugated' structure provides a pathway for electrons to move along the polymer chain. This electron delocalization occurs due to π-bonding in polymer's backbone, in which adjacent carbon atoms orbitals overlap, which are in the sp^2 P_Z configuration. This overlap enhances electron mobility throughout the polymer's backbone. In highly conjugated materials, scientists describe the electron movement using band theory, a concept borrowed from the study of traditional semiconductors.

Among the many polymers (figure 1) known to be conductive Polyaniline (PANI) [2], Poly-pyrrole (PPy) [3], Polythiophene (PT) [4], Poly(3,4-ethylenedioxythiophene) (PEDOT) [5], Poly (p-phenylene vinylene) (PPV) [6], Polyacetylene [7], Poly(3-hexylthiophene) (P3HT) [8] have been studied the most.

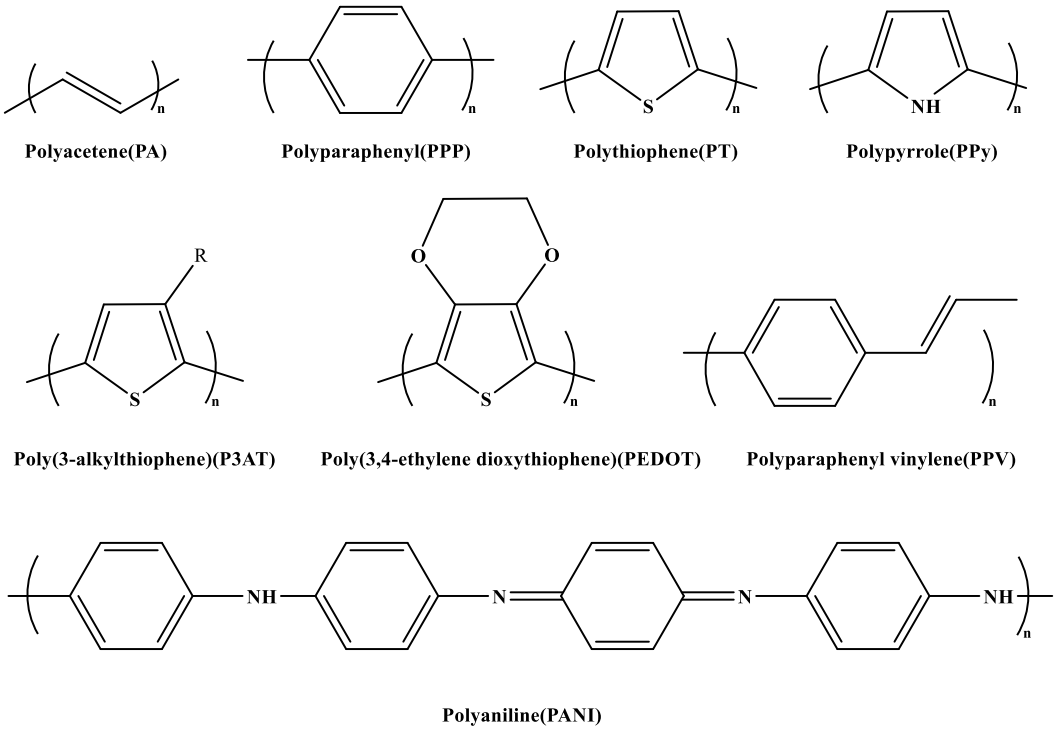

Figure 1. Chemical structures of some conducting polymers

1.1.1 Synthesis:

Conductive polymers can be synthesized using various techniques, with chemical and electrochemical polymerization being the most used methods [9].

Chemical polymerization involves linking monomers through oxidation or reduction reactions, by an appropriate oxidizing or reducing agent. Careful selection of the monomer and oxidizing/reducing agent is the key feature in this process, as these can determine the properties of the resulting polymer. For example, polyaniline is synthesized by the oxidation of aniline monomers using an oxidizing agent such as ammonium persulfate or iron (III) chloride. This process generates radical cations, which combine to form the polymer chain. Chemical polymerization is advantageous due to its simplicity, scalability, and ability to produce conducting polymers in large quantities. However, it often results in low conductivity and limited control over the polymer structure.

Electrochemical polymerization, on the other hand, offers greater control over the polymerization process. This method involves the electrolysis of a monomer solution in the presence of a conductive substrate (such as platinum or indium tin oxide). Applying an electric potential drives the oxidation or reduction of monomers at the substrate's surface, resulting in the controlled deposition of a polymer film. This process allows for better control of the polymer's properties by adjusting parameters like monomer concentration, electrolyte composition, and applied voltage.

1.1.2 Doping:

Via the doping process, an organic polymer, which is either an insulator or a semiconductor exhibiting very low conductivity, usually between 10^{-10} and 10^{1} S/cm, can be transformed into a polymer, that is in the "metallic" conducting regime (1 to 10^{4} S/cm) [10]. It can also be reversed with minimal degradation of the polymer backbone.

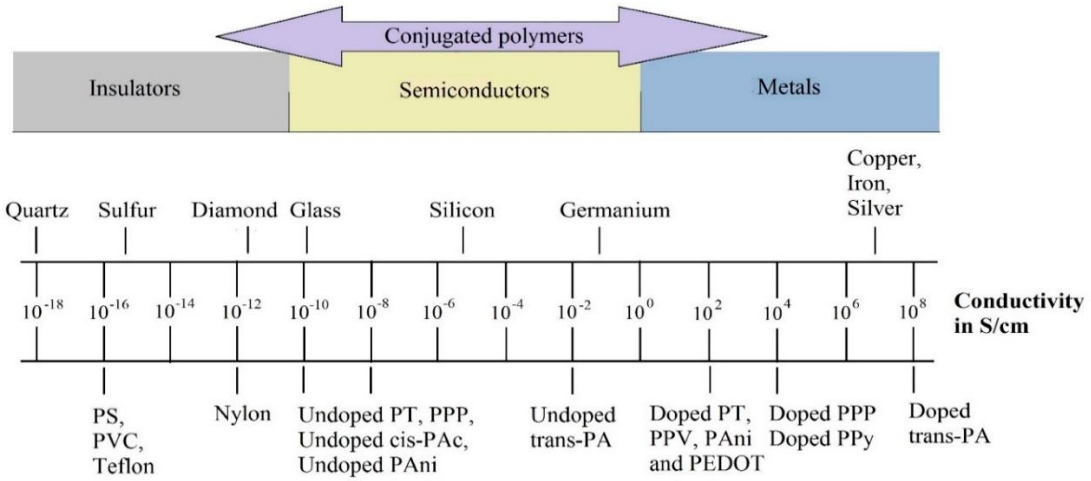

Figure 2. Conductivity of Conjugated Polymers

When conducting polymers are in their undoped state, they are typically neutral, with a fully filled valence band and an empty conduction band. This results in a large HOMO-LUMO gap, which makes these material act as an insulator. Doping introduces charge carriers into the polymer by either adding or removing electrons, reducing the HOMO-LUMO gap and allowing the material to become conductive. The doping process involves the formation of charged species, such as polarons and solitons, which support the movement of charge carriers through the material [11]. These charged species increase the transport of charge carriers along the polymer chain, which results in enhancing its conductivity. Here are a few examples of doping mechanisms in conducting polymers:

- Charge Transfer: Doping includes the transfer of charge between the dopant molecules or ions and the polymer chain, resulting in the formation of charged species within the polymer matrix.
- Polaron Formation: Doping also causes the formation of polarons, which are localized positive or negative charges along the polymer chain.
- Soliton Formation: Doping can also result in the formation of solitons, which are delocalized charges that can move along the polymer chain, contributing to the material's conductivity.

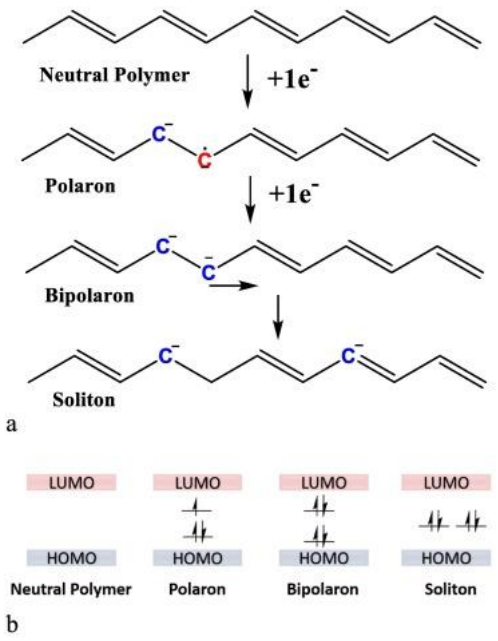

Figure 3. Polaron and Soliton formation in Conjugated polymers

Dopants in conducting polymers are generally classified into two types: p-type dopants and n-type dopants. P-type dopants accept electrons from the polymer chain, creating positively charged polarons and increasing the material's conductivity. Protonic acids like HCl and H_2SO_4 are common examples of p-type dopants. However, n-type dopants donate electrons to the polymer chain, creating negatively charged polarons and increasing the material's conductivity. N-type dopants include alkali metals like sodium and potassium.

Overall, doping can significantly affect the properties of conducting polymers, including their conductivity, stability, and optical properties. The choice of dopant can determine the type and concentration of charge carriers in the polymer chain, affecting its conductivity.

1.1.3 Applications and challenges:

Conductive polymers have applications in different fields ranging from electronics to energy storage. Their combination of electrical conductivity and mechanical flexibility makes them valuable for organic electronic devices such as OLEDs, OFETs, and OPVs [12]. However, conductive polymers face challenges in terms of stability, processability, and scalability for large-scale production. Because these materials can easily degrade due to environmental factors like moisture and oxygen, which limits their long-term performance. Additionally, the processability of conductive polymers can be difficult due to their insolubility in common solvents, which also creates problems in their structural analysis.

1.2 Chapter 2: Metal-halide Perovskites:

In recent years, metal halide perovskites (MHPs) have changed the field of materials science. These materials have a unique set of properties, including excellent optoelectronic properties, ease of fabrication, and structural tunability. Due to these excellent characteristics of these materials, researchers are focused on their many possible uses in next-generation technologies such as solar cells, light sources, sensors, and other advanced applications.

1.2.1 Structure:

Named in honour of the Russian mineralogist Lev Perovski, the term "perovskite" refers to a specific crystal structure displayed by the naturally occurring mineral, calcium titanium oxide ($CaTiO_3$). Metal halide perovskites adopt a similar structure with the general formula ABX_3 [13]:

A-site: Occupied by an organic cation like methylammonium (MA^+, $CH_3NH_3^+$) or formamidinium (FA^+, $HC(NH_2)_2^+$), or an inorganic cation like caesium (Cs^+).

B-site: A metal cation, typically lead (Pb^{2+}) or tin (Sn^{2+}).

X-site: A halide anion, such as chloride (Cl^-), bromide (Br^-), or iodide (I^-).

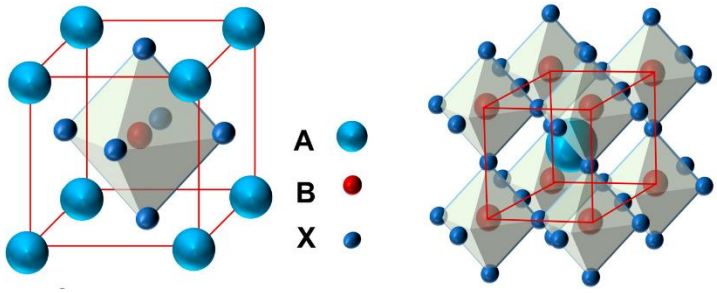

Figure 4. Structure of perovskites with ABX_3 formula

Metal halide perovskites (MHPs) are attracting attention in materials science due to their impressive light-absorbing properties, surprising tolerance for imperfections, easy fabrication, and customizable nature [14]. MHPs are very effective at absorbing a wide range of sunlight and converting it into usable electricity. Additionally, the electrical charges generated within perovskites can travel long distances, which is beneficial for efficient devices. Interestingly, unlike traditional semiconductors that are highly

sensitive to defects, MHPs still function well even with some imperfections. This forgiving nature reduces the need for extremely pure materials and complex manufacturing processes. MHPs can be prepared from solutions at relatively low temperatures, making them applicable to flexible electronics. Most importantly, the composition of perovskites can be easily modified to fine-tune their properties [15]. For example, changing the halide ratio (e.g., from bromide to iodide) in ABX_3 structure of perovskite can dramatically change the bandgap, directly affecting light absorption and emission wavelengths.

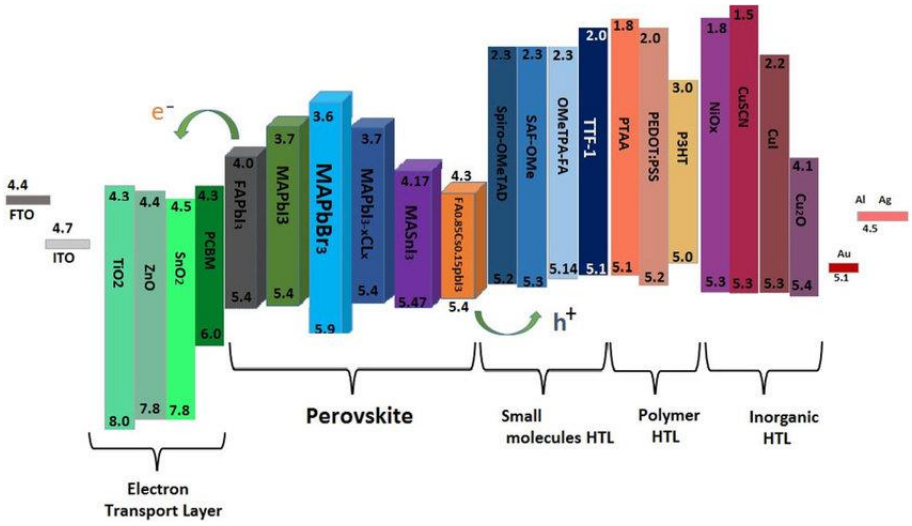

Figure 5. Schematic energy level diagram of different metal halide perovskites

Among various MHPs (figure 5), $MAPbI_3$ was the initial highlight of perovskite solar cells, boasting excellent light absorption properties and an ideal bandgap (1.55eV), driving the early breakthroughs in the field. However, researchers quickly discovered limitations in $MAPbI_3$'s thermal stability, as it degrades under typical operating temperatures (around 85℃) [16]. It also exhibits phase instability, affecting device performance. Seeking improvements, scientists turned to $FAPbI_3$ (Formamidinium lead triiodide), which has emerged as a leading candidate, particularly for photovoltaic applications due to its:

- Ideal Bandgap: $FAPbI_3$ possesses a near-optimal bandgap of 1.48eV, which is closer to the optimum bandgap value for a single-junction solar cell based on the Shockley-Queisser limit [17] and also displays a broader light absorption spectrum that extends to 840nm.
- Thermal Stability: $FAPbI_3$ exhibits higher stability at elevated temperatures compared to its methylammonium counterpart ($MAPbI_3$).

1.2.2 Challenges and Frontiers:

Despite impressive advancements, MHPs still face challenges which requires further research. One significant issue is long-term stability. Perovskite materials are prone to degradation when exposed to factors such as moisture, heat, UV light, and other environmental factors [18]. Defects within the perovskite film, particularly at grain boundaries and surfaces, can trap charge carriers and promote

non-radiative recombination (where energy is lost as heat rather than electricity). These defects also provide pathways for moisture and oxygen, accelerating degradation. Additionally, under normal conditions, the photoactive α-phase can transition into the photo inactive δ-phase, hindering its solar cell applications. Another critical challenge is lead toxicity. Research efforts are underway to identify lesser toxic alternatives to lead while preserving the high-performance characteristics of MHPs.

1.2.3 Perovskite solar cells:

Researchers began synthesizing hybrid perovskites with organic components in the 1970s, but at that time their focus was on other applications rather than solar energy. In 2009, perovskites appeared as sensitizers in dye-sensitized solar cells, with modest results (efficiency around 3.8%) [19]. A turning point came in 2012 when the use of a solid-state perovskite layer led to a significant jump in efficiency (around 9.7%) [20]. The discovery of perovskite materials for solar cell applications triggered a spike in research activity, leading to advancements in perovskite compositions, device architectures, and fabrication methods. Perovskite solar cells now demonstrate efficiencies (25.9%) [21] approaching those of traditional silicon-based technologies (26.7%) [22]. Current research focuses on enhancing their long-term stability, identifying lead-free alternatives, and developing scalable production techniques.

Overall, scientists have made incredible progress with metal halide perovskites in a very short time. In future these materials could lead to major breakthroughs in solar energy conversion and optoelectronic devices.

1.3 Chapter 3: Conducting polymer and Perovskites Hypothesis:

While perovskites demonstrate significant potential for solar cell applications, their sensitivity to moisture, oxygen, and UV radiation remains a major obstacle to commercialization [18]. Which leads to degradation pathways that compromise their long-term stability. Perovskites exhibit hydrophilic tendencies, readily absorbing moisture from the environment, which can trigger the formation of hydrates. Additionally, moisture can promote decomposition into lead salts and other organic components. Furthermore, perovskites face challenges with photostability at elevated temperatures, undergoing decomposition into lead salts. This can induce detrimental phase changes and decrease device performance.

Polymer additives offer a potential strategy to moderate these degradation mechanisms in perovskite solar cells. In this project, our core idea is to introduce a caesium salt of a conducting polymer into the perovskite material or utilize it as an interfacial layer within the perovskite solar cell. Our hypothesis on how it can interact on different levels are below:

Caesium (Cs) Component: As established, caesium itself offers benefits in mixed-cation perovskites by enhancing stability, improving phase stability, and reducing defects. Since the $FAPbI_3$ lattice has a tolerance factor of 1.03[23], it has been noted that incorporating a small percentage of methylammonium (MA^+) or caesium (Cs^+) or both helps to get the tolerance factor to be less than 1, which enhances its moisture stability.

Conducting Polymer Component: Conducting polymers provide various strategies to address the critical issue of perovskite instability, thus enhancing their viability for solar cell applications. One approach involves incorporating hydrophobic conducting polymers, such as polythiophene derivatives (e.g., P3HT), to create a protective layer that prevents moisture from infiltrating the perovskite structure. This reduces moisture-induced degradation, extending device lifespan [24]. Additionally, conducting polymers like PEDOT: PSS can passivate defects on perovskite surfaces and grain boundaries, thereby reducing unfavourable non-radiative recombination and promoting stability [25]. Careful selection of conducting polymers enables the design of interfaces that are energetically and chemically compatible with the perovskite layer. This optimizes charge extraction and minimizes degradation at the perovskite/charge transport layer junction [26]. Furthermore, certain conducting polymers can interact with perovskite precursors during crystallization, inducing nucleation and growth. This can lead to perovskite films with improved morphology, fewer grain boundaries, and enhanced stability [27].

2. Methods

2.1 Materials:

All the reagents and the solvents were purchased from BLD pharma, Avra, Sigma Alderich, TCI and Finar. Unless otherwise noted, these materials were used without further purification.

2.2 Monomer Synthesis:

To a suspension of 2,5-dihydroxy-1,4-benzenediacetic acid (2g, 8.84mmol) in anhydrous Toluene(80mL), Trifluoroacetic anhydride (TFAA)(20mL) was added. The mixture was refluxed for overnight at 60℃ upon constant stirring. Upon cooling, the volatiles were removed by using rota evaporator under reduced pressure to obtain the crude product, which was further purified by washing with hot methanol and re-crystallized from DCM to give a white crystal (1.56 g, 78%). After purification of the crude product, we obtained pure product as the Residue and pure starting material as filtrate. The white solid (Residue) was used in the next step without further purification.

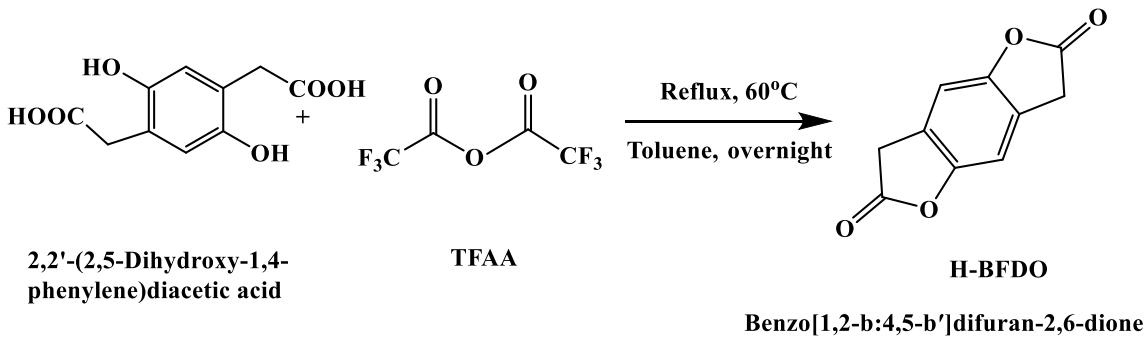

Scheme 1. Synthesis of HBFDO monomer

2.3 Synthesis of PBFDO:

At first, we synthesized PBFDO polymer by following a previously reported literature [28] using TMQ and DMSO as a reactant and further by using our own methods using HBr with DMSO and TEMPO with DMSO as a reactant.

TMQ + DMSO Method:

400 mg of H-BFDO (2.1 mmol, 1 eq.) and 518 mg of Tetramethyl quinone (3.2 mmol, 1.5 eq.) were dissolved in 25mL DMSO (extra dry) under nitrogen flow. The reaction mixture was then heated at 100 °C with continuous stirring. As the reaction progressed, the solution's colour gradually changed

from pale yellow to dark brown. After about 1 h, an increase in viscosity was observed and then the reaction mixture was allowed to cool to room temperature. After the reaction completion, to remove the DMSO from the solution, the reaction mixture was washed with Ethyl Acetate or Toluene. After drying the precipitate under vacuum, a shining black powder was obtained.

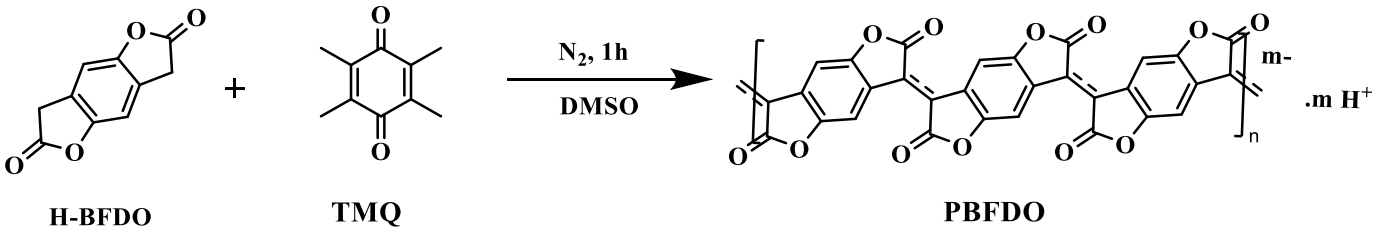

Scheme 2. PBFDO synthesis by TMQ + DMSO method

HBr + DMSO Method:

H-BFDO (50 mg, 1eq.) and HBr (140µL, 2.0 eq.) were dissolved in 5mL DMSO (extra dry) under nitrogen flow. The reaction mixture was heated at 100 °C for overnight upon constant stirring. As the reaction progressed, the solution's colour gradually changed from pale yellow to dark green. After the reaction completion, to remove the DMSO from the solution, the reaction mixture was washed with Ethyl Acetate or Toluene. After drying the precipitate under vacuum, a black powder was obtained.

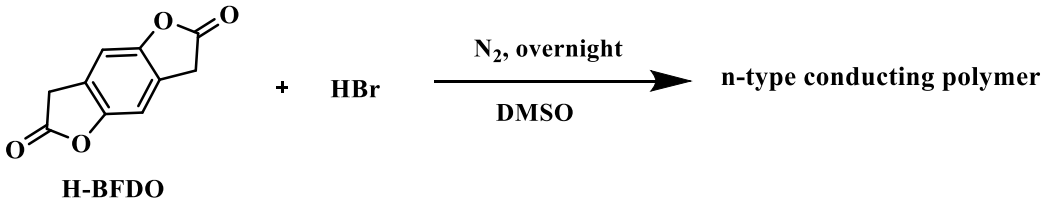

Scheme 3. PBFDO synthesis by HBr + DMSO method

TEMPO + DMSO Method:

H-BFDO (50 mg, 1eq.) and TEMPO (156 mg, 4.0 eq.) were dissolved in DMSO (15mL) under nitrogen flow. The reaction mixture was heated at 100 °C for 2h upon constant stirring. As the reaction progressed, the solution's colour gradually changed from pale red to dark brown. After about 30 min, an increase in viscosity was observed and then the reaction mixture was allowed to cool to room temperature. After the reaction completion, a very viscous gel-type solution was obtained. After the reaction completion, the reaction mixture was washed with ethyl Acetate to remove DMSO and

unreacted tempo from the mixture. After drying the precipitate under vacuum a black shining powder was obtained.

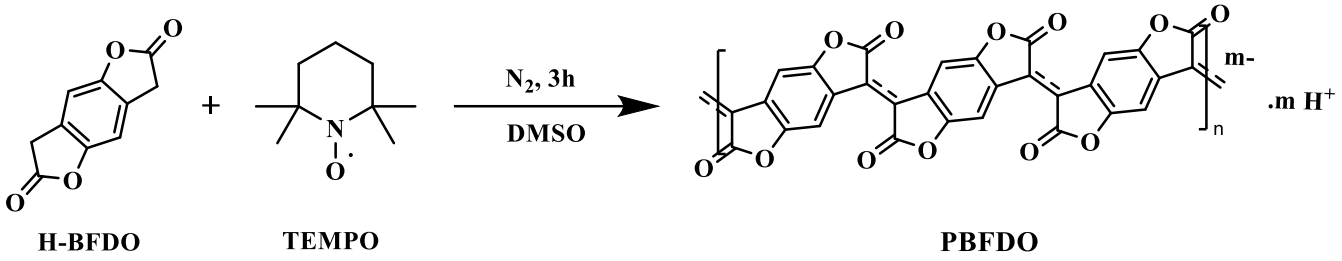

Scheme 4. PBFDO synthesis by TEMPO + DMSO method

2.4 Synthesis of Cs-PBFDO:

A mixture of 50 mg PBFDO in 15ml DMSO was prepared by continuously stirring the solution with heating it at 60 °C for 3 days. After 3 days, a gel type solution is obtained. Then in that solution, CsOH in Methanol is added dropwise to the solution and sonicated it for 30 min. We can observe the change in viscosity from gel type to solution and the colour changing from black to dark red. When the reaction is completed, we obtain a suspension of red precipitate in the reaction mixture. The reaction mixture was washed with ethyl acetate to remove the DMSO and then it was dried under vacuum at 50 °C for overnight. A very hygroscopic red powder was obtained.

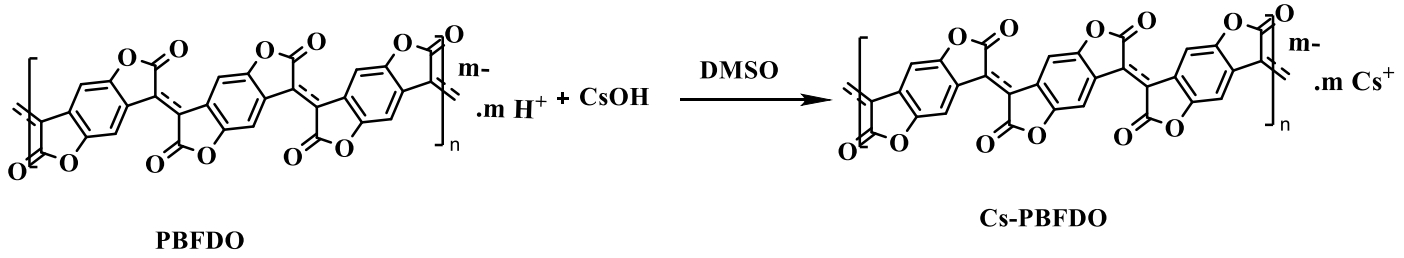

Scheme 5. Synthesis of Cs-PBFDO

2.5 Conductivity and Sheet Resistance measurements:

Electrical conductivity is a material's inherent ability to conduct electric current. It is fundamentally determined by the availability of charge carriers (electrons or holes) and their mobility within the material. Two common methods for conductivity measurement are the two-probe and four-probe techniques.

2.5.1 Two Probe Method:

Two-probe method is a simple and direct way to assess a material's electrical behaviour. Two probes (often metal electrodes) are placed in direct contact with the sample under test. Then a known current (I) is passed through the probes, and the resulting voltage drop (V) across the sample is measured. Using Ohm's Law (V = IR), the sample's resistance is calculated.

Interdigitated gold contacts photolithographically prepared on silicon dioxide (SiO_2) were used as substrate to measure the electrical conductivity of Polymer prepared by using DMSO + HBr method. The solution was drop casted on pre-cleaned substrates with the interdigitated gold contacts (figure 6). Keithley 2450 source meter was used to measure current (I)–voltage (V) characteristics.

The conductivity was calculated through the following equation: $\sigma = \frac{IL}{Vwd}$

where W is the sample width, d is the thickness of the film, and L is the span of two voltage probes.

Figure 6. Optical images of the electrode configuration of two-probe and four-probe measurements

2.5.2 Four Probe Method:

Four-probe method cleverly addresses the issue of contact resistance. In this method, four equally spaced probes are aligned in contact with the sample. The outer two probes supply a known current (I) and other inner two probes measure the voltage drop (V) across a specific part of the sample. Since the voltage-sensing probes don't carry significant current, contact resistance effects at their interface are negligible.

To measure the conductivity of the (TMQ and TEMPO method) polymer, the PBFDO solution(gel-type) was spin coated at 3000 rpm on a glass substrate having gold contacts for four probe measurement (photolithographically prepared) (figure 6).

The sheet resistance was determined by analysing the gradient of the I−ΔV curve. To ensure precise conductivity estimation, we measured the sheet resistance from multiple angles across the thin films,

alternating between the source and sense electrodes. Then the sheet resistance was calculated using the following equation:

$$R_S = \frac{\pi}{\ln 2} \times R_{avg} \approx 4.33 \times R_{avg}$$

where R_{avg} is the average resistance measured from four different directions. The conductivity of the films was then calculated by the following equation:

$$\sigma = \frac{1}{R_s t}$$

where t (film thickness) was measured by AFM.

2.6 Kelvin Probe Measurement (KPM):

Surface photovoltage measurements were done using KPTechnology Single-point Kelvin Probe system (KP020). KPM measurements were performed in an open air at room temperature, using a gold-coated Probe. A reference sample of highly oriented pyrolytic graphite (HOPG), with its known work function (4.93 ± 0.03 eV [28]), was employed to calibrate the determination of absolute work function/surface potential values. Work function (WF) of the sample can then be calculated by the following equation:

$$WF_{PBFDO}\,(eV) = WF_{tip}\,(eV) + CPD_{sample}\,(eV)$$

Here CPD is contact potential difference between the tip and the substrate

2.7 XPS Measurement:

X-ray photoelectron Spectroscopy (XPS) was performed on a PBFDO coated thin film onto an FTO substrate using a PHI 5000 VersaProbe III XPS instrument. The spectrometer utilized a monochromatic Al Kα x-ray source (approximately 100 μm spot size) with a power setting of 25 W.

2.8 General Material characterizations:

NMR spectrum was recorded on a Bruker Nano Bay 300 MHz NMR Spectrometer. 1H spectrum was referenced to the peaks of the deuterated solvent. The absorbance and transmittance of the thin films were measured by an Agilent Cary 5000 UV−vis NIR spectrophotometer. X-ray diffraction (XRD) measurements of the perovskite films were done using a Rigaku SmartLab® X-ray diffractometer.

Scanning Electron Microscopy (SEM) measurements were done using JEOL JSM 7200F FE-SEM. Single-crystal XRD measurements were done on Rigaku XtaLAB Synergy-i single crystal X-ray diffractometer. Atomic Force Microscopy (FEM) measurements were done on Nanosurf CoreAFM.

2.9 Substrate and Film preparation:

Silicon wafers and glass microscope slides underwent a rigorous cleaning protocol. This involved sequential 15-minute sonication treatments in soap, water, acetone, and isopropanol. The substrates were then dried with nitrogen and subjected to a 20-minute UV-ozone treatment (HOLMARC Ultraviolet-Ozone Cleaner). This treatment aimed to eliminate residual organic contaminants and enhance surface hydrophilicity.

2.10 PBFDO Film Preparation:

The solution of PBFDO (10 ± 2 mg ml^{-1} in DMSO) was spin coated on the pre-cleaned substrate under ambient atmosphere. The desired film thickness was precisely controlled by adjusting the spin speed. Following the coating step, the films were dried at 100 °C on a hot plate.

2.11 Fabrication of $FAPbI_3$ Perovskite Films:

A 1M $FAPbI_3$ precursor solution was prepared by dissolving formamidine hydroiodide (FAI) and lead iodide (PbI_2) in a DMF: DMSO solvent mixture (9:1 volume ratio). The desired additive quantity was incorporated, and the solution was stirred thoroughly for 4-5 hours. An antisolvent-assisted spin-coating method was used to deposit the perovskite solution onto UV-ozone treated alumina-coated glass. Spin speeds were 1000 rpm (10 seconds) followed by 6000 rpm (30 seconds). To facilitate rapid crystallization, 400 µl of ethyl acetate was applied as an antisolvent 18 seconds before the end of the spin cycle. The substrates were immediately transferred to a 150 °C hotplate for a 30-minute annealing process.

3. Results and Discussion

3.1 ^{1}H NMR spectra of H-BFDO monomer:

^{1}H NMR (300 MHz, DMSO-d^{6}, 298K): δ = 7.24 (s, 2 H, CH_2), 3.95 (m, 4 H, CH_2) ppm. And δ = 2.50 (DMSO solvent residual signal), 3.34 (H_2O in DMSO).

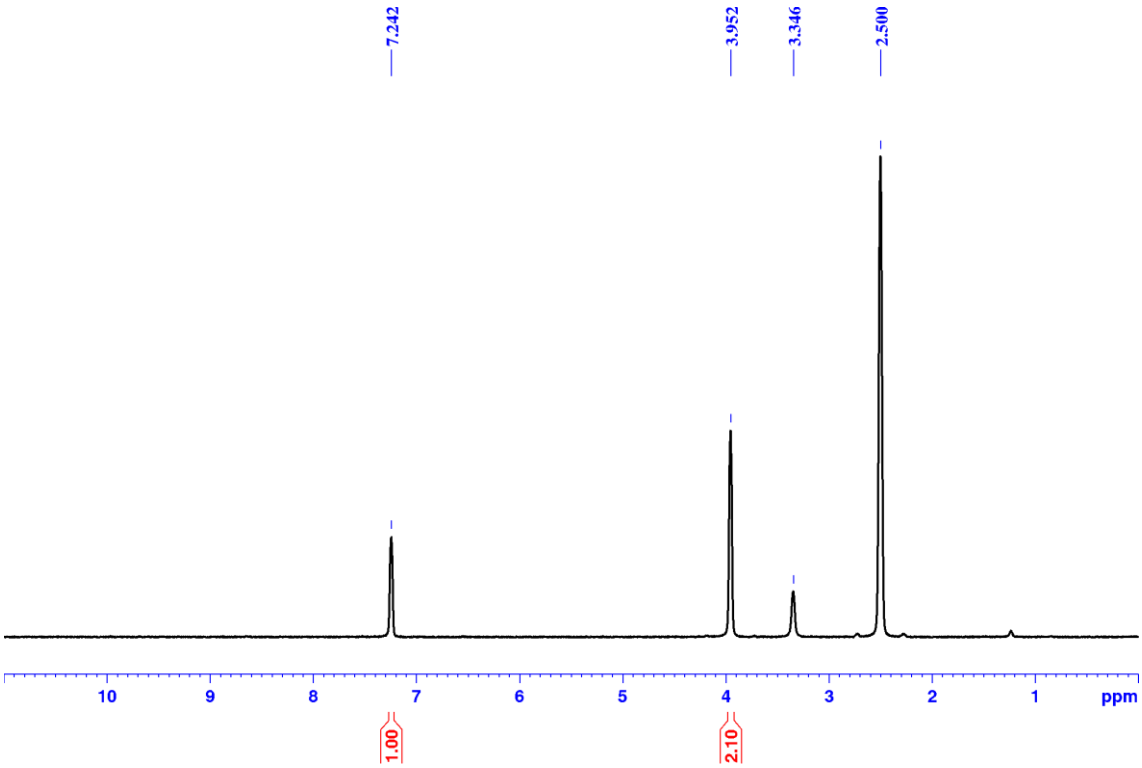

Figure 7. ^{1}H NMR spectrum of HBFDO in DMSO-d^{6} at 300 K.

Single crystals of HBFDO, suitable for X-ray diffraction analysis, were grown using an evaporative crystallization technique. A saturated solution of HBFDO was prepared in dichloromethane (DCM). This solution was then rested at room temperature overnight to allow for slow solvent evaporation. This process yielded white, well-defined crystals suitable for X-ray analysis (crystal structure presented in Figure 8).

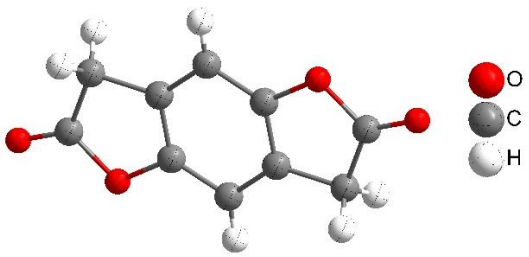

Figure 8. Crystal structure of HBFDO

3.2 Possible mechanism of TEMPO + DMSO based polymer:

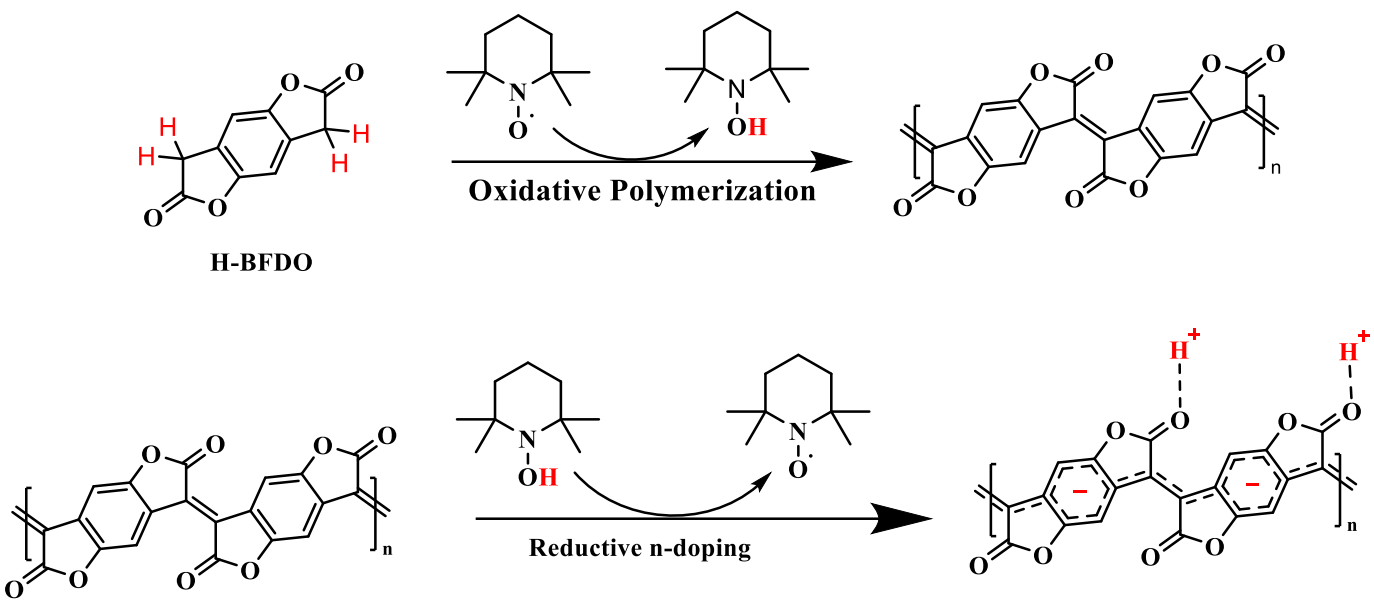

Scheme 6. Possible mechanisms of combined oxidative polymerization and reductive n-doping for the synthesis of PBFDO

3.3 In-situ NMR characterization of polymerization mechanism:

A mixture of 60 mg H-BFDO and corresponding equivalents of TEMPO were fully dissolved in 6 ml DMSO-d^6 and 0.6 ml of the mixture was charged into an NMR tube in an inert atmosphere. The mixture was heated to 100°C, and ^{1}H NMR signals were recorded at various times (See Figure 8). The gradual consumption of H-BFDO monomer (s, 7.24 ppm) and the transition from 2,2,6,6-tetramethyl-1-piperidinyloxy to 2,2,6,6-tetramethylpiperidin-1-ol (s, 7.06 ppm) were observed, confirming the oxidative process (as shown in scheme 4) in this reaction. The disappearance of monomer proton signals in the NMR spectrum after 120 min indicated reaction completion.

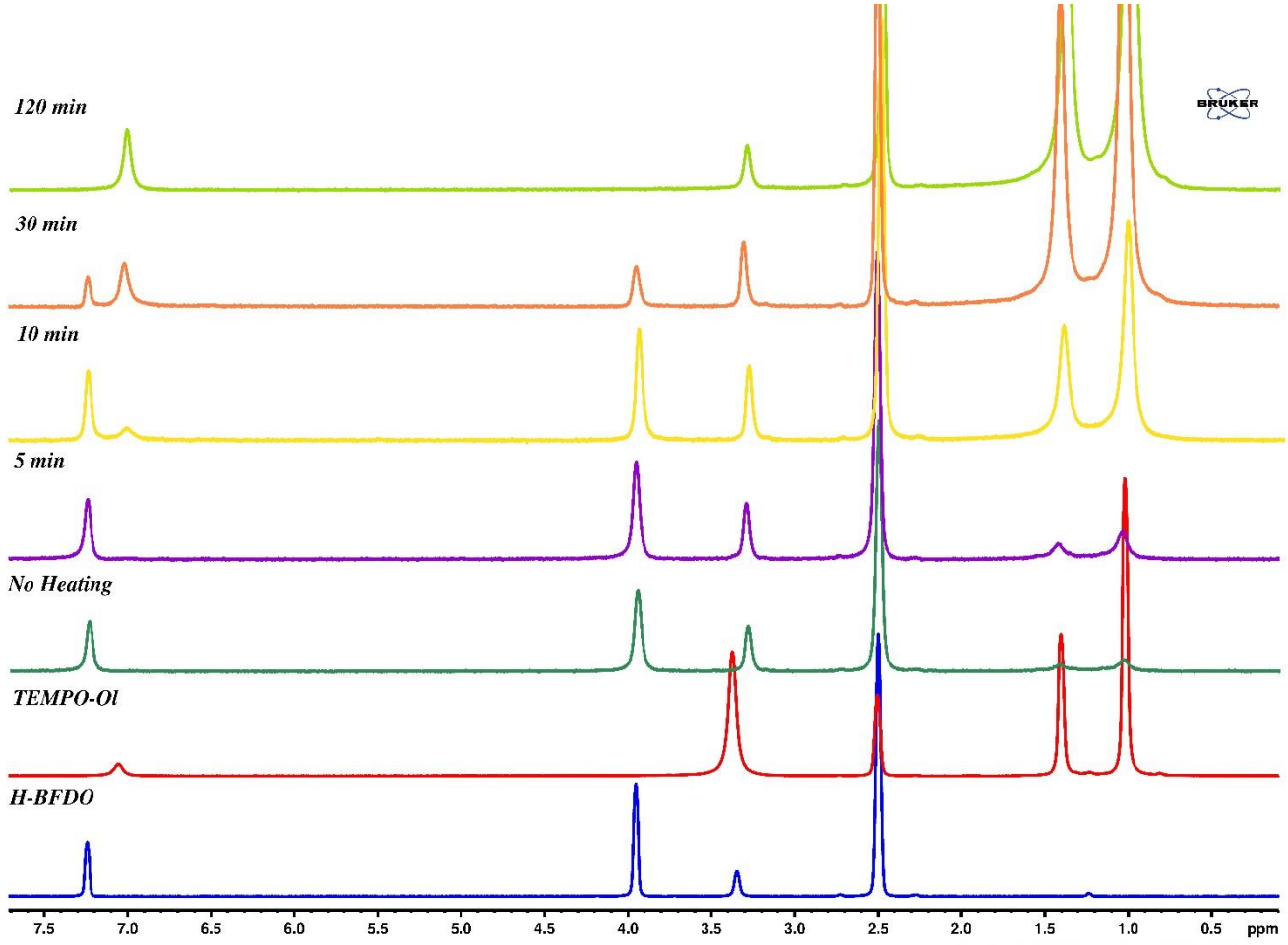

Figure 9. In-situ ^{1}H NMR monitoring of the reaction mechanism from TEMPO.

3.4 Characterization of PBFDO:

XPS measurements:

X-ray photoelectron spectroscopy (XPS) was utilized to determine the elemental composition of the film. For sample preparation, a PBFDO solution was drop casted onto an FTO-coated glass substrate and subsequently dried at 100°C for 6h. By correlating the XPS spectra with established literature values, the successful polymerization was verified. Firstly, the peak at 288.6 eV (figure 10), indicative of the H-BFDO methylene group, vanished following oxidative polymerization. Secondly, a new peak emerged at 534.7 eV in the O1s spectra, alongside with a decrease in the intensity of the carbonyl peak at 531.5 eV compared to the monomer. These spectral changes confirm the transformation of the monomeric precursor into the polymer.

H-BFDO Monomer:

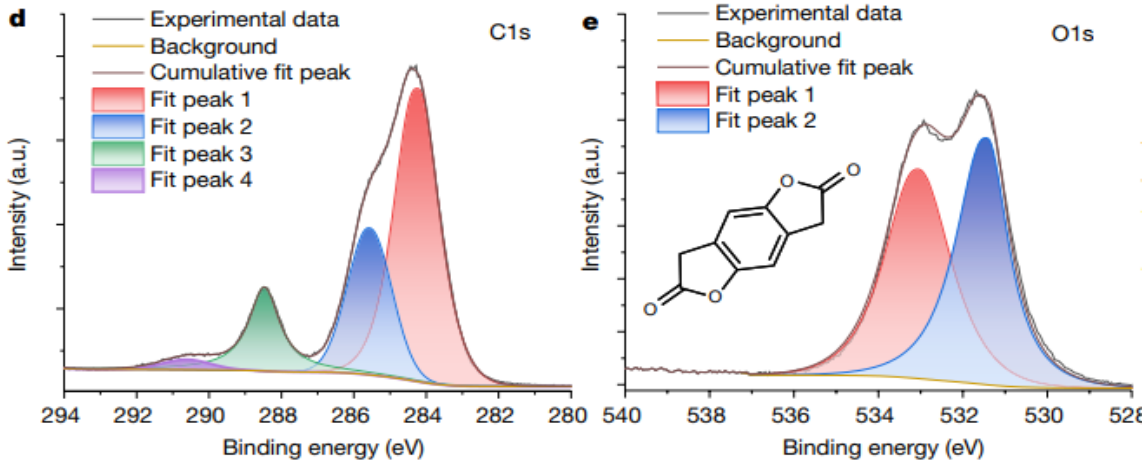

Figure 10. XPS Spectrum of HBFDO Monomer

TMQ + DMSO Method:

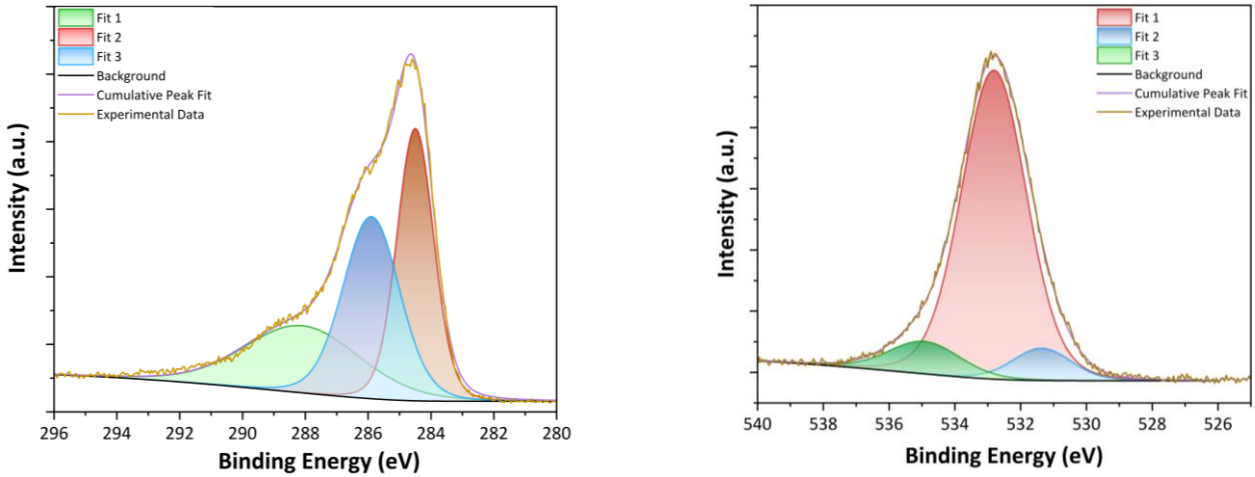

Figure 11. XPS spectrum of PBFDO polymer (TMQ + DMSO Method)

HBr + DMSO Method:

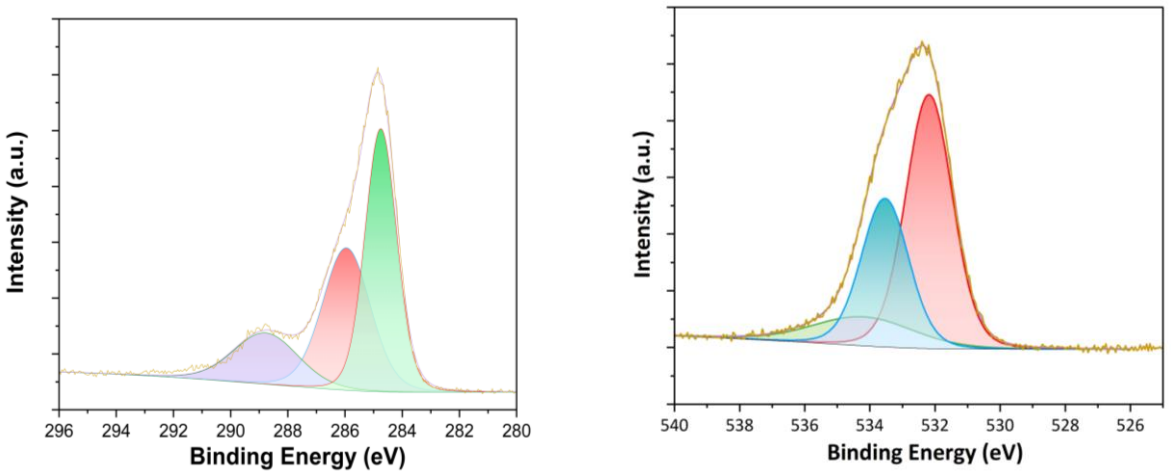

Figure 12. XPS Spectrum of PBFDO (HBr + DMSO Method)

TEMPO + DMSO Method:

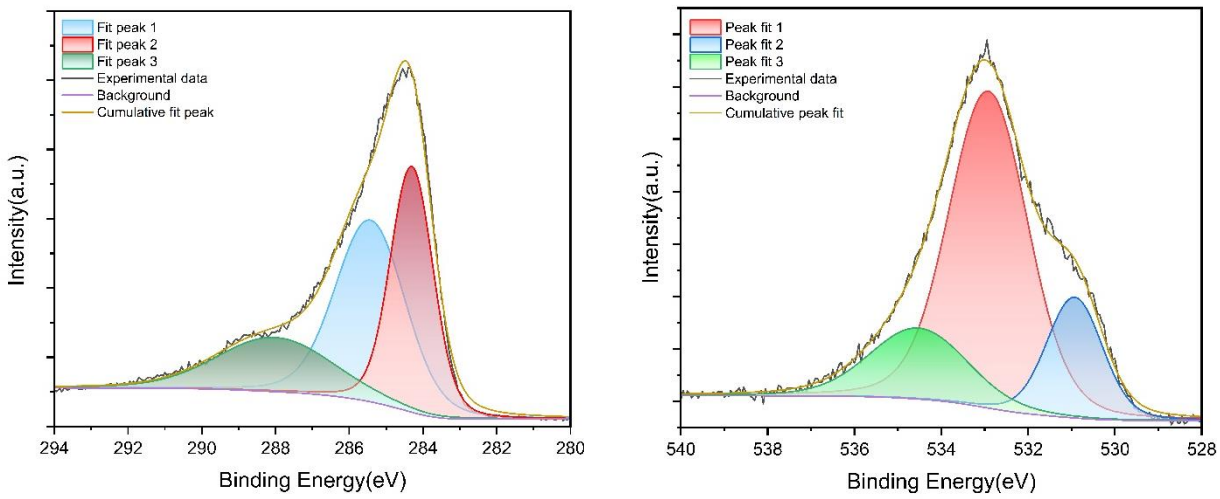

Figure 13. XPS Spectrum of PBFDO (TEMPO + DMSO Method)

Absorption Spectrum:

The PBFDO film demonstrated significant absorption extending beyond 2,000 nm (figure 14). This characteristic indicates (bi)polaron absorption, suggesting the in-situ generation of free charge carriers during the reaction process.

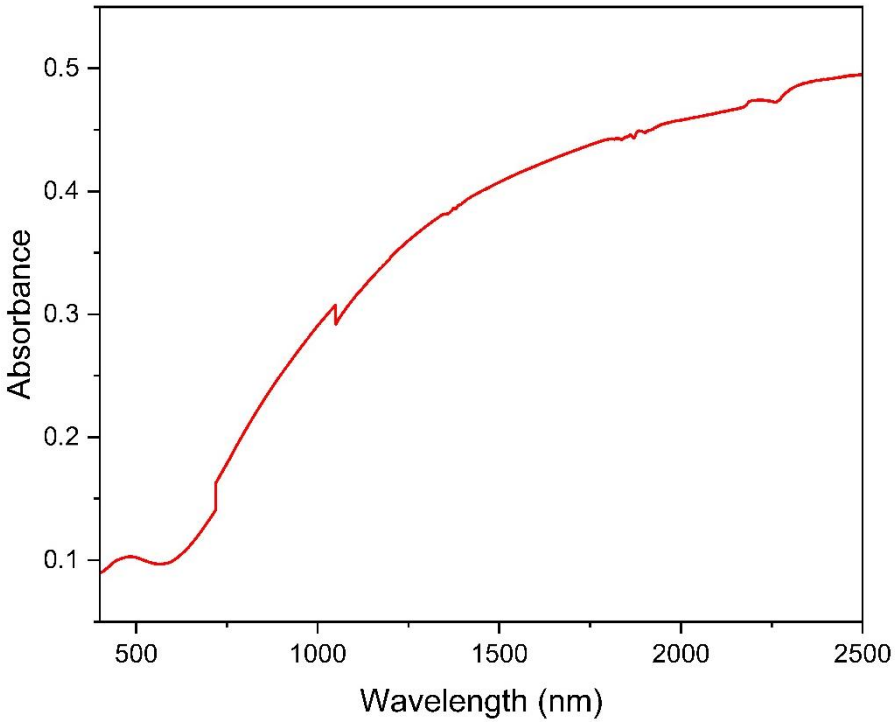

Figure 14. Absorption Spectrum of PBFDO (TEMPO + DMSO method)

Sheet resistance measurement:

Average sheet resistance for TEMPO+ DMSO method was calculated (procedure in methods section) to be around 25.22 Ω/square, while being lowest around 8.23 Ω/square at centre of the film and around 22.45 Ω/square at the near-centre and 44.96 Ω/square at the edges of the film. The PBFDO thin films for sheet resistance and conductivity measurements were coated at 3000 rpm to measure the maximum possible sheet resistance while still maintaining the transparency of the films.

Conductivity measurement:

The polymer synthesized using the DMSO + HBr method exhibited poor solubility in all tested solvents. This resulted in highly non-uniform films, due to which further characterization was not possible. Its conductivity was measured using two probe method (figure 15are)

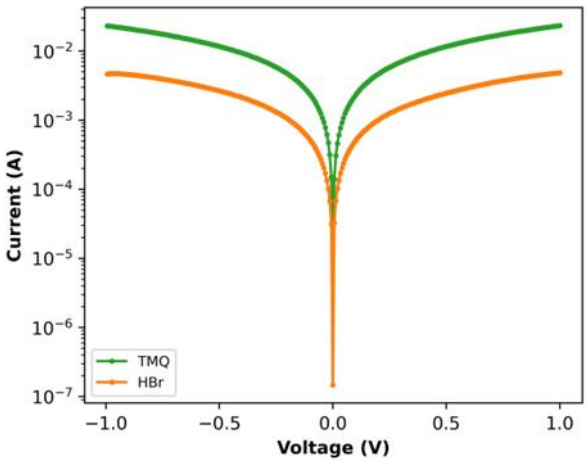

Figure 15. I-V graph of PBFDO synthesized by TMQ and HBr method

TMQ and TEMPO Methods conductivity measurements were conducted using the four-probe method (as outlined in the methods section).

TMQ + DMSO Method: A conductivity of approximately 400 Siemens/cm was determined.

TEMPO + DMSO Method: Conductivity was calculated to be around 3,706.99 Siemens/cm at the edges and 4,949.2 Siemens/cm at near-centre and 10,125 Siemens/cm at the centre of the film. So, the average conductivity of the film was measured to be 6,260 Siemens/cm. Here PBFDO thin film exhibited a thickness of approximately 120 nm at the centre and 60 nm at the edges.

AFM Measurement:

PBFDO solution (5 mg/mL DMSO) was spin-coated onto a silicon wafer substrate at a speed of 3000 rpm. Film thickness measurements were taken both at the edges and the centre of the thin film. At the edges, the thickness was determined to be approximately 60 nm (figure 16), while the central region exhibited a thickness of approximately 120 nm. The film's surface mean roughness value was calculated to be 6 nm.

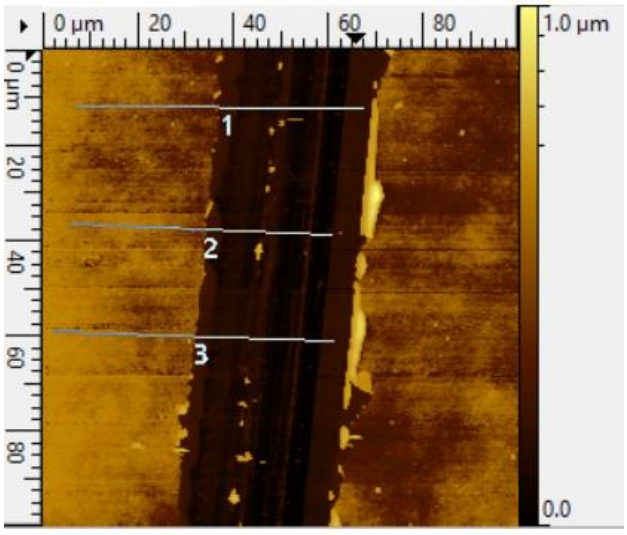

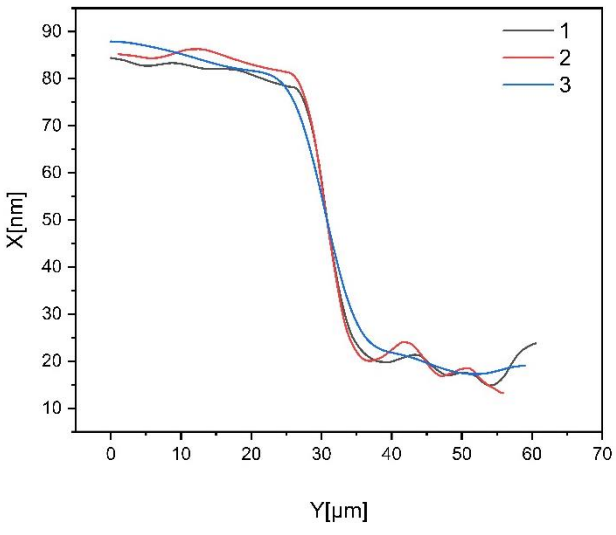

Figure 16. AFM measurement of PBFDO Thin Film

Kelvin Probe Measurement: The work function of PBFDO thin films was calculated to be 4.55 eV

3.5 Characterization of Cs-PBFDO:

^{133}Cs NMR of Cs-PBFDO:

Comparison of the ^{133}Cs NMR spectra of CsOH and Cs-PBFDO reveals a distinct peak shift (around 4.5ppm). This spectral change strongly suggests an interaction between the Cs ions and the conducting polymer matrix, supporting the formation of a Cs-polymer composite material.

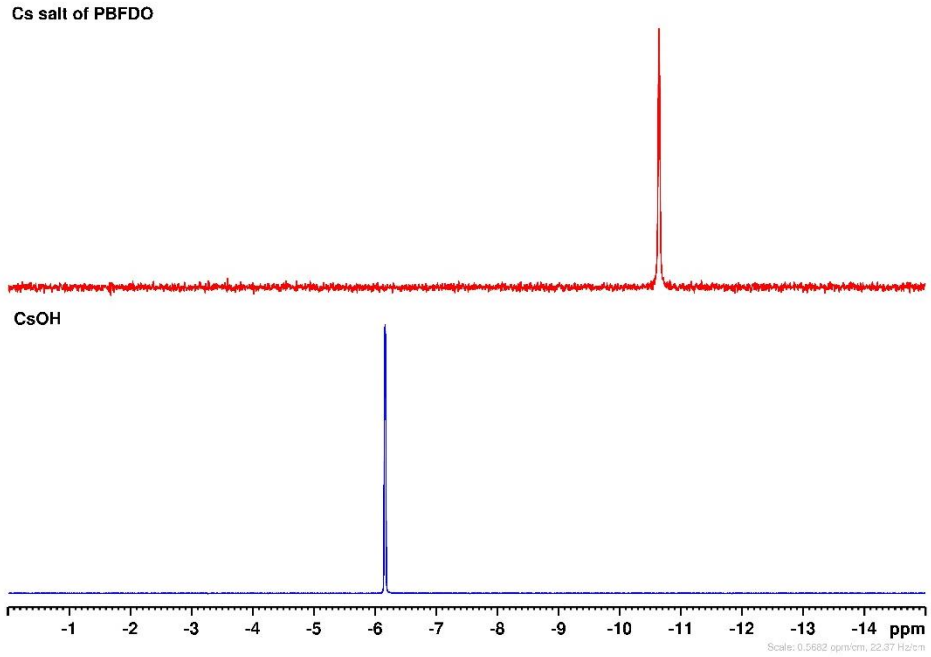

Figure 17. ^{133}Cs NMR of Cs-PBFDO and CsOH in D_2O at 300K

3.6 Investigating the Impact of Additives on $FAPbI_3$ Stability:

To address the inherent instability of $FAPbI_3$ perovskite films, we explored the potential of PBFDO and Cs-PBFDO as stabilizing additives. Three distinct precursor solutions (1M $FAPbI_3$) were prepared: a control solution without additives ("Blank"), and solutions containing 1.0 mol% of the respective additives. Following established protocols (described in method section), perovskite films were fabricated on alumina-coated glass substrates using a one-step spin-coating process.

The pure $FAPbI_3$ film transitioned to the non-perovskite delta phase within 2-3 hours after the annealing process. The addition of PBFDO offered an uncertain stability improvement, though the film degraded

within 10 days, but due to solubility issue of PBFDO polymer, the perovskite films were very patchy and non-uniform. In contrast, the Cs-PBFDO additive demonstrated a stabilizing effect. Perovskite films including this additive maintained their perovskite "black" phase for a notable duration exceeding two months. These results highlight the potential of Cs-PBFDO to significantly enhance the stability of $FAPbI_3$ perovskite films, a crucial step towards their application in real-world photovoltaic devices.

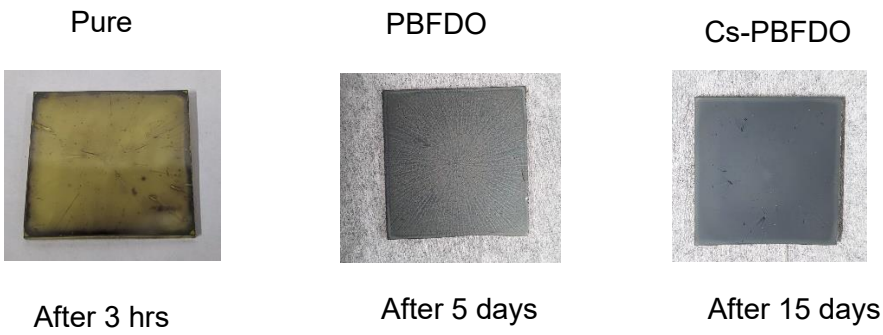

Figure 18. Optical images of pure and additive engineered $FAPbI_3$ films.

3.7 Characterization of $FAPbI_3$ with Cs-PBFDO Films:

SEM Measurements:

Perovskite films' surface morphology was investigated using top-view scanning electron microscopy (SEM) (figure 19). The film exhibited numerous pinholes, indicating need for further optimization.

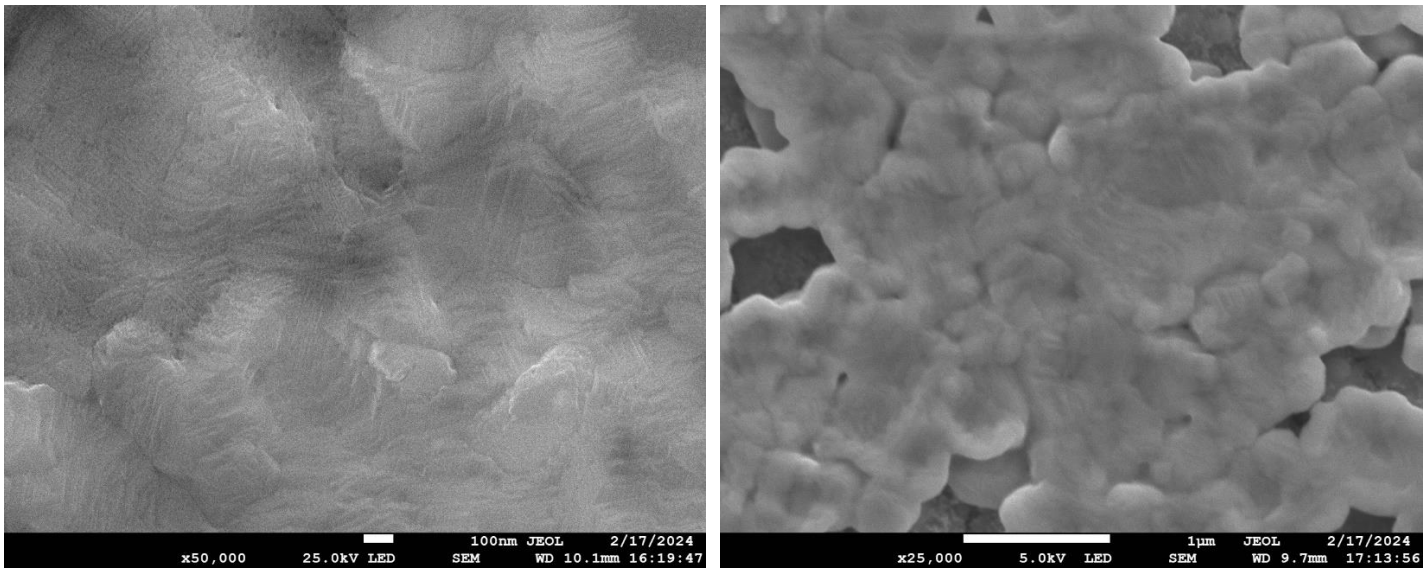

Figure 19. Top view SEM images of Perovskite Films

Absorption Spectrum and Tauc Plot of Perovskite film:

Given that, pure $FAPbI_3$ exhibits a band gap of 1.48 eV, we recorded the absorbance spectrum to assess potential changes in this value. From the Tauc plot (figure 20), assuming a direct band gap transition model, the band gap of our material was estimated to be approximately 1.483 eV. This confirms the hypothesis that our modifications in the composition of the perovskite material preserve the advantageous narrow band gap characteristic of $FAPbI_3$ perovskite.

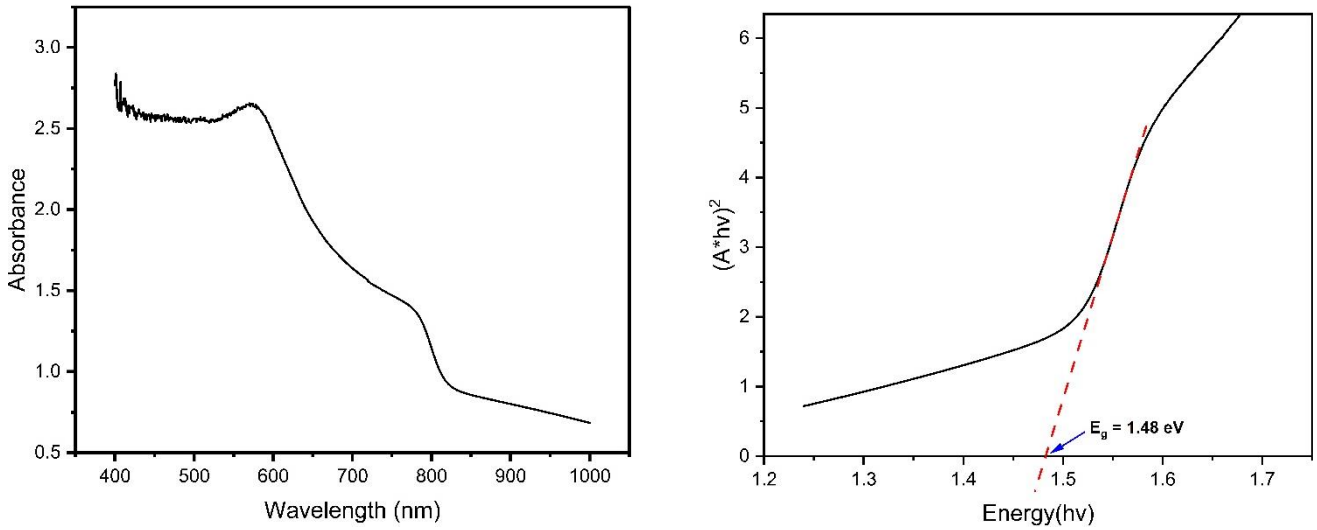

Figure 20. Absorbance spectrum and Tauc plot for 1.0 mol % added Cs-PBFDO $FAPbI_3$ film.

XRD measurements:

The diffraction peaks associated with α-FAPbI3 are 13.9°, 19.8°, 24.3°, 28.1°, 31.4°, 34.6°, 40.1°, and 42.7° and are related to (0 0 1), (0 1 1), (1 1 1), (0 0 2), (0 1 2), (1 1 2), (0 2 2) and (0 3 3) diffraction planes respectively. [30] The most intense diffraction peak for the δ-FAPbI3 is at 11.6° (0 1 0) plane and for PbI_2 are positioned at 12.6° (0 0 1). XRD data has been recorded for the 1.0 mol % added Cs-PBFDO $FAPBI_3$ film (figure 21). Where peaks labelled as (**a**) corresponds to δ-$FAPbI_3$ and peaks labelled as (**b**) corresponds to uncoordinated PbI_2 in the film.

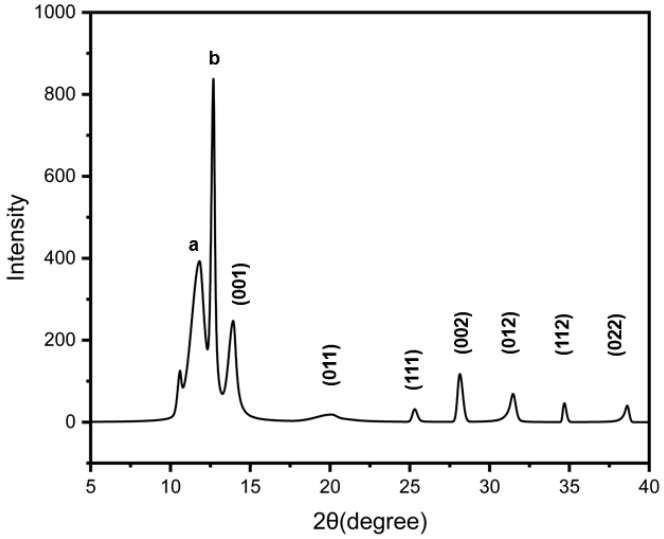

Figure 21. X-ray diffraction of thin film of $FAPbI_3$ with Cs-PBFDO additive.

The presence of pinholes and cracks in the film is resulting in the undesirable delta phase within the XRD spectrum. Further optimization is required to achieve pinhole-free and crack-free films, which will enable the formation of the pure alpha phase of $FAPbI_3$. Both XRD spectrum (figure 21) and optical images (figure 18) indicate that our additive effectively stabilizes the $FAPbI_3$ perovskite structure.

4. Conclusions:

This study established the successful synthesis and characterization of an ambient stable novel n-type conducting polymer, poly(benzodifurandione) (PBFDO). Systematic exploration of various oxidative polymerization methods (TEMPO + DMSO, TMQ + DMSO, and HBr + DMSO) revealed the TEMPO + DMSO approach as superior, yielding the highest conductivity (6260 Siemens/cm) and optimal film properties.

Advanced characterization techniques were used to get an insight into PBFDO synthesis. NMR spectroscopy provided insights into both the H-BFDO monomer structure and the TEMPO + DMSO polymerization mechanism through in-situ monitoring. XPS analysis confirmed the successful conversion of the monomer into PBFDO and offered insights into the chemical environment resulting from the different polymerization methods. Additionally, X-ray diffraction analysis explained the crystal structure of the H-BFDO monomer.

Beyond its synthesis, PBFDO demonstrated additional excellent characteristics. Kelvin probe measurements determined a work function of 4.55 eV for PBFDO thin films. And its sheet resistance was calculated to be 25.22 Ω/square while still maintaining the transparency, whereas FTO substrate has a sheet resistance around 8-10 Ω/square.

Additionally, the stabilizing potential of PBFDO as an additive for the widely studied $FAPbI_3$ perovskite was also studied. While PBFDO alone offered modest stability enhancement, incorporation of its caesium salt (Cs-PBFDO) markedly improved the stability of the $FAPbI_3$ perovskite phase. Perovskite films containing Cs-PBFDO retained the functional "black" phase for a remarkable duration exceeding two months. This finding was supported by SEM, absorbance, Tauc plot analysis, and XRD characterization. Furthermore, ^{133}Cs NMR indicated an interaction between the Cs ions and the PBFDO matrix, supporting the formation of a Cs-polymer composite.

In summary, this work demonstrates the successful development of the n-type conducting polymer PBFDO and, importantly, establishes its significant potential as a stabilizing additive for $FAPbI_3$ perovskites. This finding paves the way towards the development of more robust and efficient perovskite-based solar cells.

4.1 Future Aspects:

Further efforts are underway to optimize the conductivity and sheet resistance of PBFDO, with the goal of approaching the performance of FTO substrates. In-depth investigations into the reaction mechanism are also ongoing. The demonstrated stabilizing effect of Cs-PBFDO on $FAPbI_3$ perovskite

warrants further studies to elucidate its impact on perovskite film morphology. To achieve superior film characteristics, including the absence of pinholes, cracks, and minimized grain boundaries, additional optimization of fabrication processes is required. Ultimately, the fabrication of solar cell devices based on this material is a key objective for future research.

5. References:

[1]. Shirakawa, H., Louis, E. J., MacDiarmid, A. G., Chiang, C. K. & Heeger, A. J. Synthesis of electrically conducting organic polymers: halogen derivatives of polyacetylene, (CH)x. J. Chem. Soc. Chem. Comm. 16, 578–580 (1977).

[2] Jangid, N. K.; Jadoun, S.; Kaur, N. A. Review on High-Throughput Synthesis, Deposition of Thin Films and Properties of Polyaniline. Eur. Poly. J. 2020, 125, 109485.

[3] Jadoun, S.; Biswal, L.; Riaz, U. Tuning the Optical Properties of Poly(o-Phenylenediamine-Co-Pyrrole) via Template Mediated Copolymerization. Des. Monomers Poly. 2018, 21(1), 75–81.

[4] Senthilkumar, B.; Thenamirtham, P.; Selvan, R. K. Structural and Electrochemical Properties of Polythiophene. Appl. Surf. Sci. 2011, 257(21), 9063–9067.

[5] Ouyang, L.; Kuo, C.; Farrell, B.; Pathak, S.; Wei, B.; Qu, Martin, D. C. Poly [3, 4-Ethylene Dioxythiophene (Edot)-co-1, 3, 5-Tri [2-(3, 4-Ethylene Dioxythienyl)]-Benzene (Eph)] Copolymers (Pedot-co- eph): Optical, Electrochemical and Mechanical Properties. J. Mater Chem. B. 2015, 3(25), 5010–5020.

[6] Erdur, S.; Yilmaz, G.; Goen Colak, D.; Cianga, I.; Yagci, Y. Poly (Phenylenevinylene) as Sensitizers for Visible Light Induced Cationic Polymerization. Macromolecules. 2014, 47(21), 7296–7302.

[7] Chien, J. C. W.;. Polyacetylene: Chemistry, Physics, and Material Science; Elsevier: London, 2012.

[8] Kim, J. S.; Park, Y.; Lee, D. Y.; Lee, J. H.; Park, J. H.; Kim, J. K.; Cho, K. Poly(3-hexylthiophene) Nanorods with Aligned Chain Orientation for Organic Photovoltaics. Adv. Func. Mater. 2010, 20(4), 540–545.

[9] Pan, L.; Qiu, H.; Dou, C.; Li, Y.; Pu, L.; Xu, J.; Shi, Y. Conducting Polymer Nanostructures: Template Synthesis and Applications in Energy Storage. Int. J. Mol. Sci. 2010, 11(7), 2636–2657.

[10] Kar, P.; Doping in Conjugated Polymers; John Wiley & Sons: Hoboken, NJ, 2013.

[11] Ribeiro, L. A.; Monteiro, F. F.; da Cunha, W. F.; E Silva, G. M. Charge Carrier Scattering in Polymers: A New Neutral Coupled Soliton Channel. Sci. Rep. 2018, 8(1), 1–7.

[12] Facchetti, A.; π-Conjugated Polymers for Organic Electronics and Photovoltaic Cell Applications. Chem. Mater. 2011, 23(3), 733–758.

[13] Fan, Y.; Meng, H.; Wang, Li.; Pang, S. Sol. RRL 2019, 3, 1900215.

[14] De Wolf, S. et al., J. Physics. Chem. Lett. 2014, 5, 1035-1039.

[15] Zhou, C.; Lin, H.; Chaaban, M.; He, Q.; Xu, L.; Lee, S.; Shi, X.; Ma, B. Mater. Sci. Eng. 2019, 137, 35.

[16] N.-K. Kim, Y.H. Min, S. Noh, E. Cho, G. Jeong, M. Joo, S.-W. Ahn, J.S. Lee, S. Kim, K. Ihm, H. Ahn, Y. Kang, H.-S. Lee, D. Kim, Investigation of thermally induced degradation in $CH_3NH_3PbI_3$ perovskite solar cells using in-situ synchrotron radiation analysis, Sci. Rep. 7 (2017) 4645.

[17] W.Shockley, H.J. Queisser, Detailed balance limit of efficiency of p-n junction solar cells, J. Appl. Phys. 32 (1961) 510e519.

[18] Yi, Z.; Ladi, N. H.; Shai, X.; Li, H.; Shen, Y.; Wang, M. Nanoscale Adv., 2019, 1, 1276 1289.

[19] A. Kojima, K. Teshima, Y. Shirai, T. Miyasaka, Organometal halide perovskites as visible-light sensitizers for photovoltaic cells, J. Am. Chem. Soc. 131 (2009) 6050e6051.

[20] Kim, H.-S.; Lee, C.-R.; Im, J.-H.; Lee, K.-B.; Moehl, T.; Marchioro, A.; Moon, S.-J.; Humphry-Baker, R.; Yum, J.-H.; Moser, J. E.; Gratzel, M.; Park, N.-G. Lead Iodide Perovskite Sensitized All Solid-State Submicron Thin Film Mesoscopic Solar Cell with Efficiency Exceeding 9%.

[21] M.A. Green, E.D. Dunlop, J. Hohl-Ebinger, M. Yoshita, N. Kopidakis, A.W.Y. Ho-Baillie, Solar cell efficiency tables (Version 55), Prog. Photovoltaics Res. Appl. 28 (2020) 3e15.

[22] Lin H et al. 26.7% efficiency silicon heterojunction solar cells achieved by electrically optimized 10 nanocrystalline-silicon hole contact layers. 1–23 (2023).

[23] Kim, G.; Min, H.; Lee D. Y.; Seok, S. Science 2020, 370, 108-112.

[24] Li, X., Zhang, W., & Wang, Y. (2020). Enhancing perovskite solar cell stability with P3HT hole transport layer. Solar Energy Materials and Solar Cells, 215, 110659.

[25] Chen, H., & Yang, S. (2019). Defect passivation in perovskite solar cells using PEDOT: PSS. ACS Applied Materials & Interfaces, 11(35), 31535-31543.

[26] Zhou, Y., Yang, M., & Snaith, H. J. (2018). Interfacial engineering of perovskite solar cells with PCBM. Materials Horizons, 5(1), 26-34.

[27] Liu, T., Chen, K., Chen, Q., Peng, J., & Li, L. (2021). Controlled crystallization of perovskite films with PTAA for enhanced stability and performance of solar cells. Journal of Materials Chemistry A, 9(32), 17602-17611.

[28] Tang, H., Liang, Y., Liu, C. et al. A solution-processed n-type conducting polymer with ultrahigh conductivity. Nature, 611, 271–277 (2022).

[29] Harima Y, Yamashita K, Ishii H, Seki K (2000) Energy structures of molecular semiconductors contacting metals under air studied by the diffusion potential measurements and the Kelvin probe technique. Thin Solid Films, 366:237–248.

[30] Murugadoss, G., Arunachalam, P., Panda, S. K., Kumar, M. R., Rajabathar, J. R., Al Lohedan, H., & Wasmiah, M. D. Journal of materials research and technology, 2021, 12, 1924-1930.